IMPACT OF JUNCTION BREAKDOWN IN MULTI-CRYSTALLINE SILICON SOLAR CELLS ON HOT SPOT FORMATION AND MODULE PERFORMANCE

Fabian Fertig, Stefan Rein, Martin Schubert and Wilhelm Warta
Fraunhofer Institute for Solar Energy Systems (ISE)
Heidenhofstrasse 2, 79110 Freiburg, Germany
Phone: +49 761 4588 5656, Fax: +49 761 4588 9250, Email: fabian.fertig@ise.fraunhofer.de

ABSTRACT: Localized diode breakdown in mc-Si solar cells is suspected to be potentially critical to module encapsulation when occurring during the operation of a shaded solar cell in reverse. By modelling the operating point of two model cells under varying shading conditions, we show that every cell, breaking down or not, can suffer from significant power dissipation in a standard industrial module. We discuss, that early breakdown can even be beneficial concerning worst case total power dissipation in a shaded cell and module output power. Experimentally, we show that type I, II and III breakdown sites which were identified by DLIT and EL on solar cells from umg and virgin-grade feedstock have not led to critical hot spot temperatures. However, a newly observed edge effect which was activated at approximately 160°C after a significant shading time severely damaged the investigated module. Partial shading of solar cells revealed that the dark part of a cell, even when exhibiting the dominant breakdown mechanism during full shading, can be dominated by the illuminated part, which is supported by modelling a partially shaded cell with a parallel connection of a fully shaded and a fully illuminated cell.
Keywords: Module, Shading, Modelling, Multi-crystalline Silicon, Diode Breakdown

1 INTRODUCTION

If a solar cell is shaded in a photovoltaic module by e.g. leaves, bird droppings or snow, it can be reverse-biased to voltages up to $V_{rev} \approx -15$ V depending on module architecture and can therefore dissipate up to approximately a third (for 3 incorporated bypass diodes) of the module's maximum output power. When being locally concentrated, this power dissipation can lead to hot spots damaging solar modules irreversibly. Figure 1 depicts an example of the backsheet of an industrial module being severely damaged by an arising hot spot.

In multi-crystalline silicon (mc-Si) solar cells, reverse voltages in this regime can lead to localized electrical junction breakdown [1] causing localized heating. The breakdown sites are categorized into three types with different characteristics [2]: "Type I" breakdown is suspected to arise from paste remnants on the wafer surface [3], "type II" is attributed to metal precipitates [4] and "type III" to etch pits showing an avalanche-like breakdown behaviour [5]. Hence, "type III" breakdown depends on the base resistivity of the wafer but is suspected to be avoidable in principle by adapting wet chemical processes. However, also "type II" breakdown which is correlated to material properties has been shown to depend on the base resistivity leading to lower breakdown voltages for lower base resistivities [6]. Due to doping compensation, wafers crystallized from umg feedstock usually exhibit lower base resistivities than wafers crystallized from virgin-grade feedstock. Hence, umg mc-Si solar cells usually break down at lower reverse voltages even when exhibiting comparable metal impurity concentrations. The effect of decreased junction breakdown voltage in umg mc-Si solar cells is critical for industrial acceptance of umg Si and is one of the main reasons hindering a wider use of umg feedstock in industrial production although an efficiency potential similar to virgin feedstock has been shown [7].

Previous work on hot spots mainly focused on two aspects: the physical origin of junction breakdown in mc-Si solar cells (e.g. [1]-[6]) and the hot spot effect in modules without tracing the origin to specific localized defects on cell level (e.g. [8, 9]). This work is bringing both aspects together: First, the operating conditions of shaded solar cells with different characteristics are simulated to predict the power dissipation under different shading scenarios for a standard module architecture with and without bypass diodes. It is shown, that the total power dissipation in a shaded solar cell is only moderately limited by bypass diodes. For partial shading conditions, a simple model is applied to separate dark and illuminated part of the cells with respect to power dissipation. To determine the locally resolved power dissipation, mc-Si solar cells are fabricated from virgin-grade and umg-Si feedstock and intensively characterized. Conclusively, these cells are assembled into a module and tested on hot spots. Furthermore, the related module output power loss due to different shading scenarios is addressed.

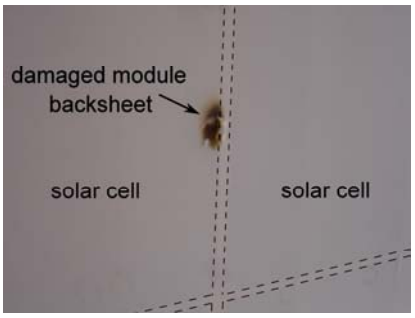

Figure 1: Module backsheet damaged by a hot spot.

2 MODULE OPERATION WITH SHADED CELLS

The following theoretical discussion focuses on two aspects: (1) the behaviour of a standard module's output power with shaded cells and, more importantly, (2) the operating point and power dissipation of shaded cells in a standard module. Aspect 1, i.e. the output power behaviour of a solar module with shaded cells is well understood and broadly discussed in literature (e.g. [10]-[13] and many more). However, aspect 2, i.e. determining the exact operating point and its implications for junction breakdown in shaded mc-Si solar cells, has not been addressed in detail so far to the author's knowledge. A principle overview on the calculation procedure is given in [10] and a basic discussion with simplifying

approximations for the case of a shaded cell without junction breakdown in a solar module with bypass diodes is published in [11]. Furthermore, the difference in the operating point of a shaded cell is discussed for two scenarios: (i) the solar module operating under short-circuit conditions (= worst case scenario which is, e.g., tested during certification in the so-called hot spot endurance test [14, 15]) and (ii) the module operating at its altered maximum power point are discussed.

For this purpose, two model cells (cells A and B) are considered, which are incorporated into a standard industrial module consisting of a series connection of 60 solar cells (a configuration which is broadly applied for cells with 156 mm edge length), which are divided into strings by three bypass diodes that are connected in parallel to 20 cells each. Alternatively, the model module shall also be operated without bypass diodes.

2.1 Model cells and module

The shaded model cells discussed in the following are described via the two-diode model of a solar cell [16] which is modified by a term adapted from Bishop [10] (similarly to [11]) for a more accurate description of a cell's reverse behaviour. The JV characteristic is given by

$$J = J_{ph} - J_{01}e^{\frac{V+R_sJ}{n_1V_t}} - J_{02}e^{\frac{V+R_sJ}{n_2V_t}} - \frac{V+JR_s}{R_p}\left(1+a\left(1-\frac{V+R_sJ}{V_b}\right)^{-b}\right). \quad (1)$$

Cells A and B shall exhibit identical forward bias behaviour which is described by the parameters dark-current saturation densities $J_{01} = 1$ pA/cm^2 and $J_{02} = 1$ nA/cm^2, ideality factors $n_1 = 1$ and $n_2 = 2$, for diodes 1 and 2, respectively as well as series resistance $R_s = 0.5$ Ωcm^2 and parallel resistance $R_p = 3$ kΩcm^2 (thermal voltage $V_t(25°C) = 25.69$ meV). However, the cells shall exhibit a different reverse bias behaviour which is described by the parameters [10, 11] correction factor $a = 0.05$, avalanche breakdown exponent $b = 1.1$ and junction breakdown voltage $V_b = -16$ V for cell A and $a = 0.5$, $b = 1.1$ and $V_b = -9.5$ V for cell B. The area of both cells is $A_{cell} = 15.6 \times 15.6$ cm^2.

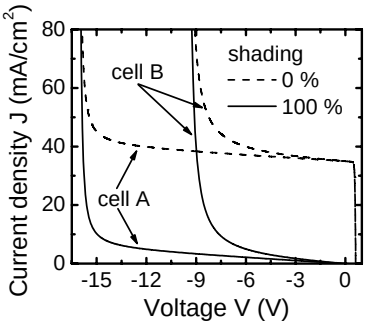

Figure 2: Illuminated and dark JV characteristics of model cells A and B. Parameters see text.

Figure 2 shows the resulting illuminated (photo-generated current $J_{ph,cellA} = J_{ph,cellB} = J_{ph,max} = 35$ mA/cm^2) and dark JV characteristics of cells A and B. Note, that the focus lies on the reverse voltage range of the cells. Hence, the forward bias range is comparably small on the displayed scale. Cell B represents a mc-Si cell with an early junction breakdown and cell A a mc-Si cell with a later junction breakdown. The other 58 cells incorporated into the discussed module exhibit the same forward bias parameters as cells A and B. Additional series resistance of cell interconnectors is neglected here but can easily be added into the model.

2.2 Module behaviour for fully and partially shaded cells

2.2.1 Full shading

Without incorporated bypass diodes, the discussed module is a series connection of multiple cells, therefore the resulting IV characteristic of different cells can be gained by summing their voltages at a set current value [10, 17]. With incorporated bypass diodes, the module current value is the sum of the currents through an individual string and the bypass diode (BPD) connected in parallel to it. With a set string current, the string voltage can be calculated which equals the negative value of the voltage across the BPD connected to it. This gives the current through the BPD and the sum of string and BPD current is the current going into the other strings. Iterating this procedure by sweeping the string current gives the module's IV characteristic [10].

First, it is assumed that no bypass diodes are incorporated into the module. Figure 3a shows the module IV characteristic without any cells being shaded and the resulting module IV characteristic with cell A being fully shaded. Without bypass diodes, the altered module characteristic follows the reverse characteristic of the shaded cell due to the series connection. On the left hand side of Fig. 3a, the voltage applied to the shaded cell A is depicted over the module current. Without bypass diodes, the module current equals the string current which flows through the shaded cell. The voltage across the shaded cell and the module IV curve therefore follow the behaviour of cell A depicted in Fig. 2. It can be seen, that cell A breaks down for module output voltages smaller than approximately 20 V. Multiplying voltage and current leads to the output power of the module ($P_{module} = V_{module} \times I_{module}$) and the power being dissipated in the shaded cell ($P_{cell} = V_{shaded\ cell} \times I_{string}$), see Fig. 3b. The behaviour of P_{cell} over module output voltage V_{module} is gained as follows: each module output voltage V_{module} gives a module current I_{module}, see right hand side of Fig. 3a. This module current gives the voltage applied to the shaded cell $V_{shaded\ cell}$, see left hand side of Fig. 3a. Since without bypass diodes, the module current equals the string current I_{string} flowing through the shaded cell, the product of $V_{shaded\ cell}$ and $I_{module} = I_{string}$ gives P_{cell}. Figure 3b shows, that the maximum output power of the module significantly decreases from $P_{module} = 256$ W without shading to $P_{module} = 126.5$ W for cell A being fully shaded and without incorporated bypass diodes. The maximum possible power dissipation in cell A is up to $|P_{cell}| = 134$ W.

If bypass diodes are incorporated, the voltage applied to a shaded cell under reverse bias is limited to

$$\left|V_{rev}\right|_{\max} \le \left(\sum_{i=1}^{cells/string-1} V_{cell_i} + V_{bypass\,diode}\right). \quad (2)$$

Hence, the voltage applied to cell A during module operation saturates once the BPD gets conductive and cell A does not break down entirely, see left hand side of Fig. 3a. At the same time, the BPD conducts the additional current generated by the other two strings of the module while the current through the string containing cell A (which equals the current through cell A) saturates, see Fig. 3c. Hence, the power being dissipated in cell A ($P_{cell} = V_{shaded\ cell} \times I_{string}$) saturates once

the BPD turns on, see Fig. 3b, which leads to a significantly lower maximum possible power dissipation of $|P_{cell}| = 15.5$ W than without incorporated bypass diodes. In the module output characteristic, the turn-on of the BPD leads to a steeper increase of the module current compared to the case without incorporated bypass diodes, see Fig. 3a, and hence a higher maximum power output of the module of $P_{module} = 165.5$ W, see Fig. 3b. Therefore, for cell A the maximum module output power is increased and maximum power dissipation in the shaded cell decreased under full shading conditions when bypass diodes are incorporated.

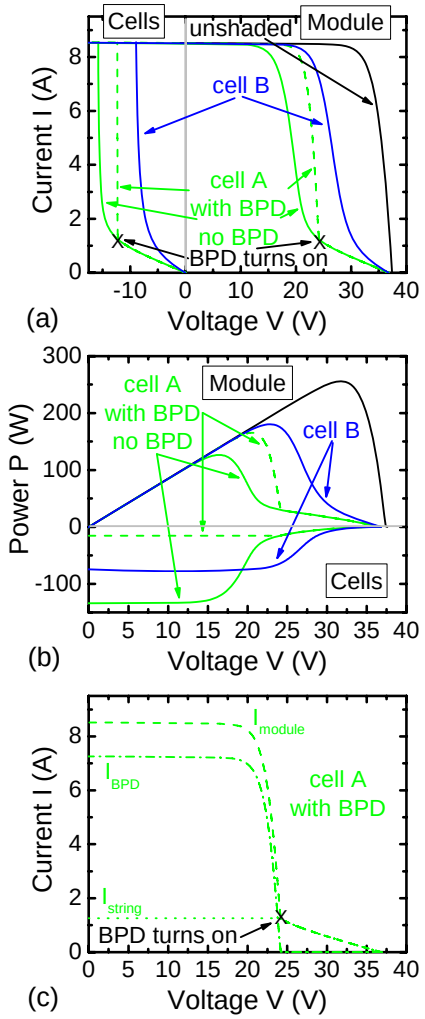

Figure 3: (a) Module IV characteristics unshaded (black) and with cells A (green) and B (blue) being fully shaded respectively (right hand side) and voltage applied to cells A (green) and B (blue) respectively over module current (left hand side). (b) Module PV characteristics according to scenarios in (a). (c) Module, string and BPD currents for cell A being fully shaded.

If cell B is fully shaded, the module characteristic follows the cell characteristic analogously to the case of cell A being fully shaded and no bypass diodes being incorporated, see Fig. 3a. On the left hand side of Fig. 3a, it can be seen, that the negative voltage across cell B does not get to the point where the BPD is turning on. Hence, the entire module current flows through cell B at every operation point. Whether bypass diodes are incorporated into the module or not, does neither affect module output power nor the power dissipated in cell B. Therefore, cell B breaks down for module output voltages smaller than approximately 28 V independently of whether bypass diodes are incorporated or not.

Compared to cell A with a higher break-down voltage, fully shading cell B leads to a higher maximum module output power of $P_{module} = 180.5$ W. With a worst case power dissipation of $|P_{cell}| = 76.5$ W, fully shading cell B leads to a higher value than fully shading cell A with incorporated bypass diodes but to a lower value than fully shading cell A without incorporated bypass diodes, see Fig. 3b.

2.2.2 Partial shading

If one part of a cell is shaded and another part of the same cell is illuminated at the same time, this scenario is called partial shading. As a measure for the amount of shading, the shading ratio is introduced as

$$R = \frac{A_{dark}}{A_{cell}} 100. \qquad (3)$$

For both cell A and B, a uniform photo-generated current density of $J_{ph,cellA} = J_{ph,cellB} = J_{ph,max} = 35$ mA/cm^2 is assumed in the illuminated part of the cell. Hence, the effect of partial shading is modelled by calculating the resulting photo-generated current of the cell by weighting the current density with the applied shading ratio. For example: Shading half a cell leads to $I_{ph,50\%\ shading} = 0.5 \times I_{ph,max} = 4.26$ A with $I_{ph,max} = 15.6 \times 15.6$ cm$^2 \times 35$ mA/cm$^2 = 8.52$ A. This is equivalent to the case, that the entire cell is shaded by a semi-transparent object leading to a transmission of 50 % of the incident radiation only. Figure 4a shows the resulting illuminated module IV characteristics for cell A being shaded at different ratios with and without incorporated bypass diodes. The lower the shading ratio, the higher is the resulting photo-generated current of the partially shaded cell. This shifts the reverse characteristic of cell A and hence the resulting module characteristic to higher currents.

The resulting power-voltage (PV) characteristics are depicted in Fig. 4b. For 75 % shading, the behaviour is similar as for the case of 100 % shading, i.e., at the maximum power point of the module cell A is negatively biased and by incorporating bypass diodes the maximum output power of the module increases while the maximum power dissipation in cell A decreases. For 50 % shading, the behaviour is similar if bypass diodes are incorporated. However, without bypass diodes the maximum power point of the module is in a voltage regime where cell A (50 % shaded) operates under positive bias and still contributes to the module's output power. Hence, at the maximum power point, cell A does not dissipate power although half the cell area is shaded. For 25 % shading, this is the case for both bypass diodes being incorporated and not being incorporated. Hence, the power dissipation in a partially shaded cell at the maximum power point of the module can significantly differ from the worst case of the module being short-circuited which is usually tested.

Figure 4b also shows, that even with incorporated bypass diodes, power dissipations of more than $|P_{cell}| = 80$ W are possible in a partially shaded cell, which exhibits a low current under full shading at the point of bypass diode turn-on. Analogously to Fig. 4a and b, cell B can be considered as well.

Figures 5a and b show the resulting maximum power

output of the module as a function of shading ratio if cells A and B are partially shaded, respectively. For higher shading ratios of cell A, the bypass diode limits the loss in maximum module output power compared to the case without incorporated bypass diodes. Figure 5d illustrates the effect discussed for the case of 50 % shading in Fig. 4b in more detail. For shading ratios smaller than 45 %, cell A is operated under positive bias and contributes to the output power at the maximum power point of the module (P_{cell} = 0 to 4.3 W under forward bias, i.e. very small on the used scale in Fig. 4b). Hence, the BPD is not turned on and thus does not make a difference in maximum module output power, see Fig. 5a. For higher shading ratios (more than 45 % with bypass diodes, more than 60 % without bypass diodes), the maximum power point of the module shifts to the regime where cell A is being reverse biased and does not contribute to the output power of the module anymore. This turn-over point occurs at lower shading ratios when bypass diodes are incorporated as illustrated by the case of 50 % shading in Fig. 4b.

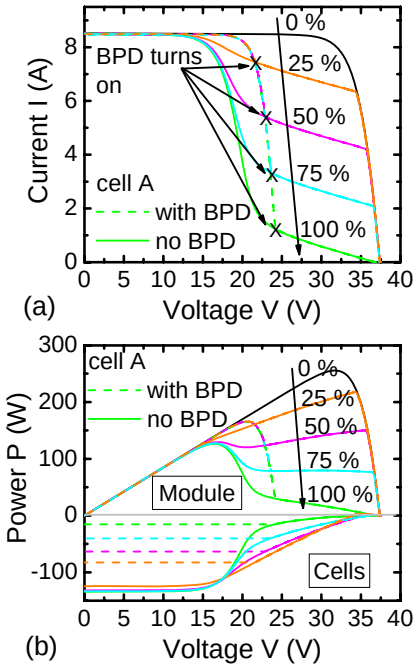

Figure 4: (a) Module IV characteristics with cell A being shaded by different ratios. (b) Module PV characteristics according to scenarios in (a).

If both cells contribute to the module's output power, which is the case for shading ratios smaller than 40 %, the maximum module power output is identical due to the identical forward bias behaviour of cells A and B, see Fig. 5a and b. However, as indicated in Fig. 3b for the full shading case of cell B, partially shading cell B leads to a lower loss in maximum module output power than shading cell A once cell B does not contribute to the module's output power anymore (as expected for cells with lower breakdown voltages than the voltage necessary for the BPD to turn on). This is the case for shading ratios greater than 40 % as shown in Fig. 5f.

The worst case scenario for power dissipation in partially shaded cells is when the module is being short-circuited. In this regime, a partially shaded cell with identical forward bias behaviour as the other cells in the module always dissipates power. Figures 5c and e depict the resulting total power dissipation in cells A and B. For cell B, the power dissipation decreases with decreasing shading ratio; the reason is, that the voltage applied in reverse to cell B (Fig. 5u) which is necessary to supply the module's short-circuit current (which itself equals the current through cell B, see I_{total} in Fig. 5q) decreases with increasing photo-generated current in cell B (also indicated in Fig. 2). In other words, the portion of the photo-generated current does not need to be generated by driving cell B in reverse bias. Hence, a lower reverse voltage is sufficient to supply the difference between $I_{ph,cell}$ and I_{total}. Since the voltage applied in reverse to cell B is too small for bypass diodes to turn on, see left hand side of Fig. 3a, the entire short-circuit current of the module always completely flows through cell B. Per definition cell B therefore represents a current-limited cell for the discussed module architecture, also referred to as "type B cell" in module certification norms [14, 15]. The behaviour for cell A is qualitatively identical if no bypass diodes are incorporated, see Fig. 5c. Since the necessary voltages to supply the module's short-circuit current are higher for cell A than for cell B due to cell A's later junction breakdown (see Fig. 2 and 5s), the power dissipation is higher in cell A.

If bypass diodes are incorporated, the total power dissipation behaviour in cell A is significantly different, see Fig. 5c. The dissipated power increases for decreasing shading ratios (starting from 100 %), because the current through cell A increases due to the photo-generated current as can be seen by I_{total} in Fig. 5o, while the voltage across cell A only changes very little because it is limited according to Eq. 2, see Fig. 5s. Per definition cell A therefore represents a voltage-limited cell for the discussed module architecture, also referred to as "type A cell" in module certification norms [14, 15]. The total power dissipation increases down to a shading ratio of 15 %. At this point, the non-shaded cells in the string including cell A operate close to their maximum power point and the entire power is dissipated in cell A. Further decreasing the shading ratio leads to a lower power dissipation again because, analogously to the case without incorporated bypass diodes, a lower voltage applied in reverse to cell A is necessary to supply the module's short-circuit current due to the increasing photo-current, see Fig. 5s. As soon as the voltage across cell A falls below the necessary value for the bypass diode to significantly conduct current, the behaviour with and without incorporated bypass diodes becomes identical which is the case for shading ratios below 15 %.

Comparing partial shading behaviour under short-circuit conditions (tested during IEC and UL certification) for cells A and B (Fig. 5c and e) reveals, that depending on shading ratio the maximum total power dissipation in a voltage-limited cell (i.e. late junction breakdown) can be higher than in a current-limited cell (i.e. early junction breakdown) even in the case of incorporated bypass diodes. In other words: In a standard module with incorporated bypass diodes, cell A, that does not get into the reverse bias regime of hard junction breakdown during shaded operation and that exhibits values of $I_{cellA,dark}$(-10 V) = 0.93 A and $I_{cellA,dark}$(-12 V) = 1.2 A, suffers from a higher worst case power consumption than cell B, that operates in the reverse bias regime of hard junction breakdown (with and without incorporated bypass diodes) and conducts the module's short-circuit current of $I_{sc,module}$ = 8.52 A at a

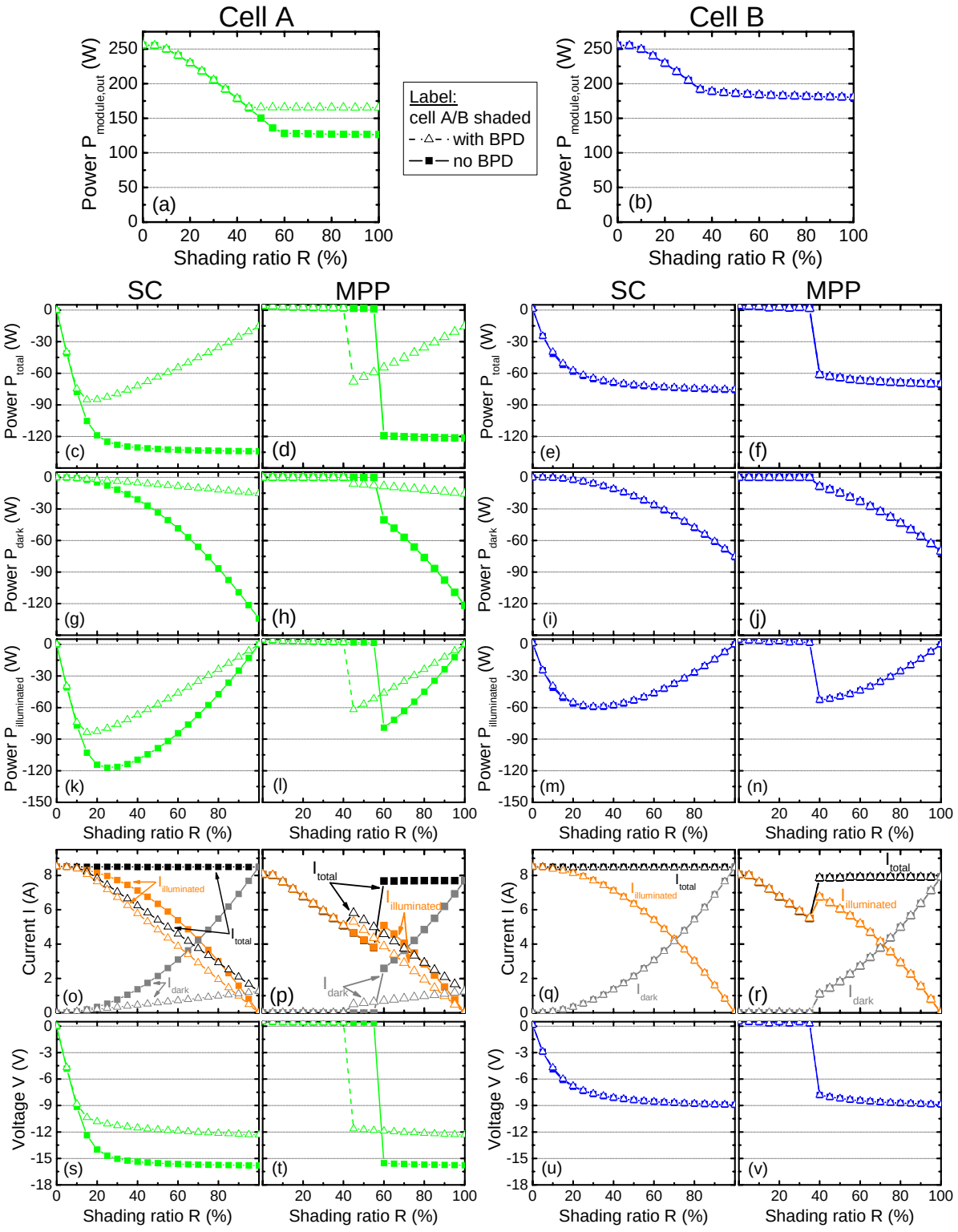

Figure 5: Various cell and module characteristics as a function of the shading ratio for **(left half)** partial shading of cell A (with later junction breakdown) and **(right half)** partial shading of cell B (with earlier junction breakdown) shown in both cases under short-circuit conditions (1st and 3rd column) and under maximum power conditions (2nd and 4th column) of the module. The characteristics are calculated for a module with bypass diodes (open symbols) and without bypass diodes (closed symbols).
(a)+(b) Maximum module output power (see Fig. 4b). **(c)-(f)** Total dissipated power in partially shaded cell (see Fig. 4b). **(g)-(j)** Dissipated power in dark the part of the partially shaded cell. **(k)-(n)** Dissipated power in the illuminated part of the partially shaded cell. **(o)-(r)** Total current flow through the partially shaded cell and individually for the dark and the illuminated part. **(s)-(v)** Applied voltage to the partially shaded cell

.

voltage of $V_{cellB,dark}$ (8.52 A)= -8.94 V already.

Comparing the total power dissipation in cells A and B under short-circuit conditions (see Fig. 5c and e) and at the module's maximum power point (see Fig. 5d and f), respectively, shows that the qualitative behaviour is comparable once the cells operate in reverse bias, see the applied voltages to the cells in Fig. 5s-v. For cell A without incorporated bypass diodes and for cell B, the quantitative values of the total dissipated power are lower at the module's maximum power point than under short-circuit conditions because $I_{MPP,module} < I_{sc,module}$, see I_{total} in Fig. 5p and r compared to Fig. 5o and q (the voltages in reverse are slightly lower as well but negligible towards the difference in current, see Fig. 5t and v compared to Fig. 5s and u). For cell A with bypass diodes being incorporated, the power dissipation under short-circuit conditions and at the maximum power point are practically identical once cell A is operating under reverse bias because both voltage (see Fig. 5s and t), and current (see Fig. 5o and p), are pinned by the turn-on point of the bypass diode and $I_{string} = I_{cellA} < I_{MPP,module}$ for shading ratios greater than 45 %.

2.2.3 Circuit model for the separation of dark and illuminated part of a partially shaded cell

To investigate the behaviour of a partially shaded cell in more detail, a simple model is applied to describe the illuminated and dark part of a partially shaded cell separately. Figure 6 shows the equivalent circuit: A partially shaded cell is described by the parallel connection of a fully shaded and a fully illuminated cell. Quaschning [11] has shown that this model (two diodes) gives approximately equivalent results as the model applied in subsection 2.2.2 (one diode) for modelling a partially shaded solar cell under forward bias. Here, the model is expanded to determine the power dissipation in the different parts of a shaded cell under reverse bias. To simulate the dark and illuminated part separately, both parts are described by the modified two-diode model according to Eq. 1. The voltage applied to the partially shaded cell is calculated analogously to subsection 2.2.2, see Fig. 5s-v and the current via

$$I_{cell} = J_{dark} \cdot A_{dark} + J_{illuminated} \cdot A_{illuminated} = I_{dark} + I_{illuminated}$$

with $A_{dark} = A_{cell} \cdot$ shading ratio / 100

and $A_{illuminated} = A_{cell} - A_{dark}$.

Simulating the total power dissipation shown in Fig. 5c-f yields the same results for both models which confirms the applicability of the new model also under reverse bias. The following discussion is again based on the model cells A and B with the characteristics of the dark and illuminated parts of the cells according to Fig. 2 with $J_{ph,dark} = 0$ mA/cm^2 and $J_{ph,illuminated} = J_{ph,max} = 35$ mA/cm^2, respectively.

Figures 5g-n reveal how (according to this simple model) the total power dissipation in the partially shaded cell, shown in Fig. 5 c-f, is distributed between the dark and illuminated part of the cells. First, cell B shall be considered under short-circuit conditions of the module, which is displayed in Fig. 5i and m. For decreasing shading ratio starting from 100 %, the constant total current is continuously shifted from the dark part of the cell to the illuminated part (see Fig. 5q), while the necessary voltage in reverse to supply the module's short-circuit current slowly decreases (see Fig. 5u) due to the increasing photo-current being generated in the illuminated part of the cell. Hence, the dissipated power in the dark part of the cell (Fig. 5i) decreases while the dissipated power in the illuminated part increases (Fig. 5m). For shading ratios smaller than 30 %, the decrease in necessary voltage to supply the required current outweighs the increase in photo-generated current leading to a decrease in the power dissipation in the illuminated part of the cell again. Under short-circuit conditions of the module, cell A again behaves qualitatively similarly to cell B if no bypass diodes are incorporated with the reverse voltages and therefore the dissipated power values being higher, as can be seen in Fig. 5g, k, o and s.

In the case that cell A is partially shaded with incorporated bypass diodes, the global current increase with decreasing shading ratio starting from 100 % is only due to the photo-generated current in the illuminated part of the cell (see Fig. 5o). Hence, the power dissipation in the illuminated part of the cell increases while the power dissipation in the dark part decreases from a low level already. Since the voltage applied to cell A in reverse is pinned by the bypass diode and not the entire short-circuit current of the module needs to be supplied by the cell only, the maximum power dissipation in the illuminated part occurs at a slightly lower shading ratio than for the case without bypass diodes.

For the comparison between the behaviour at the maximum power point of the module and the module under short-circuit conditions, the same relations are valid as discussed for the behaviour of the total cell, see subsection 2.2.2.

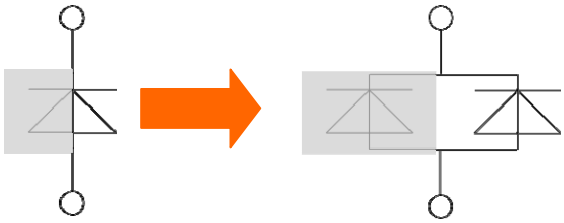

Figure 6: Applied model for a partially shaded cell.

2.4 Summary module modelling

To sum the theoretical discussion up, the following points shall be emphasized again:

(1) The main effect of bypass diodes is to limit the output power loss of a solar module with a shaded cell to approximately the power of one string. However, bypass diodes only limit the worst case total power dissipation in a shaded cell to approximately the maximum power of one string which for the case of a standard industrial module with 3 strings with 20 cells each is in the order of $P_{total,max} = 85$ W. That is, every cell that does not break down before incorporated bypass diodes turn-on (explicitly including cells with very low currents in the dark at the operating point in a module with integrated bypass diodes) dissipates the maximum possible power of its entire string (here: $P_{total,max} = 85$ W) for a specific shading ratio.

(2a) In a "good" cell with low current under reverse bias in the dark at the point of the bypass diode to turn on the worst case power dissipation is higher than or equal to the worst case power dissipation in a "bad" cell with a high current under reverse bias in the dark. It is equal if the "bad" cell is still voltage-limited and higher if the "bad" cell is already current-limited. For cells with different reverse characteristics, the worst case power

dissipation occurs at different shading ratios.

(2b) Prevention of junction breakdown by bypass diodes does not always limit total power dissipation in a solar cell. Cells with earlier breakdown can even have a lower worst case maximum power dissipation than cells with a higher breakdown voltage depending on the shading ratio.

(3) Junction breakdown at reverse voltages lower than the voltage required to turn on incorporated bypass diodes can result in smaller power losses of a solar module during shading even though incorporated bypass diodes never turn on.

(4) For current-limited cells, bypass diodes neither make a difference in maximum module output power nor maximum power dissipation in the shaded cell under standard operating conditions. They can therefore be omitted.

(5) Maximum power dissipation is expected in the illuminated part of a partially shaded cell.

(6) The operating point of a solar cell under certain shading conditions can be predicted for a given reverse characteristic and module architecture and hence the probability of different breakdown mechanisms to occur for different shading scenarios.

Not discussed are the points of varying irradiation level and temperature, but by adapting the cell parameters accordingly, the resulting module and cell behaviour can easily be predicted.

3 EXPERIMENTAL

To investigate the impact of junction breakdown on hot spot formation, a test module was manufactured.

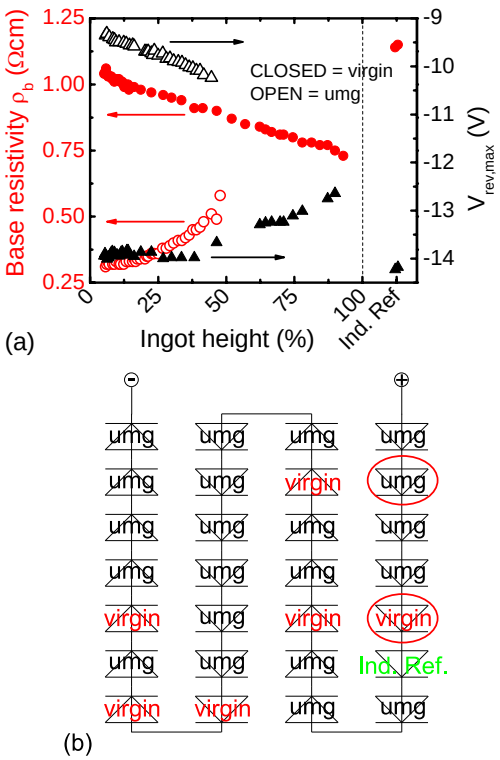

Figure 7: (a) Dependence of base resistivity (circles) and breakdown voltage (triangles) on ingot height for two mc-Si crystals from umg (open symbols) and virgin-grade (closed symbols) feedstock. (b) Schematic of assembled test module.

3.1 Test module

The entire fabrication process of the test module starting from commercially available umg and hyper-pure, virgin-grade feedstock was conducted on industrial equipment at Fraunhofer ISE [18, 19]. Two ingots were crystallized, wafered and processed into industrial standard Al-BSF solar cells.

Figure 7a shows the base resistivity measured inductively and the reverse voltage that is necessary to conduct a current of 10 A in the dark, $V_{rev,max}$, as a function of ingot position for solar cells manufactured from the two crystallized ingots and for solar cells manufactured from reference virgin-grade industrial mc-Si wafers. The umg wafers cover a resistivity range from ρ_b = 0.3 to 0.6 Ωcm which increases over ingot height due to doping compensation and the virgin-grade wafers from ρ_b = 0.7 to 1.1 Ωcm which decreases over ingot height due to the segregation of boron which is the only dopant. The breakdown voltages are in the range from $V_{rev,max}$ = -9.3 to -10.2 V for the umg cells and from $V_{rev,max}$ = -12.6 to -14.9 V for the virgin-grade cells. The breakdown voltage behaves inversely proportionally to the base resistivity over ingot height which confirms the findings of Kwapil et al. [6] and Wagner et al. [20].

The cells were intensively pre-characterized by means of IV measurements, dark lock-in thermography (DLIT) and electroluminescence (EL). Moreover, to roughly estimate the hot spot potential of the cells under steady-state conditions, which represents the situation when being shaded in a module, the cells were reverse biased and local heating being monitored by a temperature-sensitive thermofoil which gets damaged at temperatures T < 50°C. None of the cells incorporated in the module caused damage to the thermofoil. (Note, that within the measurement setup the cells are placed on a copper chuck for the rear side contact which exhibits significantly different thermal characteristics than the encapsulation system of a solar module. However, very critical cells can be identified since they lead to instant damage of the thermofoil.) Subsequently, selected cells were built into a test module using industrial equipment at Fraunhofer ISE. To ensure breakdown of all investigated cells upon shading, 28 cells are connected in series to supply the necessary voltage for reverse biasing the shaded cells under test. No bypass diodes were incorporated. Figure 7b depicts the schematic of the assembled test module.

3.2 Exemplary test cells

One virgin-grade cell (ρ_b = 0.75 Ωcm, $V_{rev,max}$ = -12.6 V) and one umg cell (ρ_b = 0.34 Ωcm, $V_{rev,max}$ = -9.6 V) are discussed in more detail in the following. Figure 8a shows the dark reverse IV characteristics of the two cells recorded in an industrial cell tester; Fig. 8b the module characteristics measured in the thermal chamber where the module is tested on hot spots ($T_{module} \approx 50°C$) for different shading scenarios: (i) unshaded, (ii) each of the two cells being 100 % shaded and (iii) the umg cell being partially shaded. As expected from the simulations, the module IV characteristic under full shading follows the shaded cells' reverse characteristics. The slope in the top part of the unshaded module IV curve is due to strong mismatch between the incorporated cells, not due to some sort of shunting.

Figures 9e and j show the spatially resolved on-set voltages of the virgin-grade and the umg cell,

respectively. Both topographies are derived from a series of DLIT images under reverse bias. The on-set voltage is defined as the voltage from which a point on the cells carries a significantly higher current than a "dark" grain that does not contribute to the reverse current flow. If the locally increased current is due to junction breakdown, these images correlate well to the breakdown maps derived from EL images recorded under reverse bias. Comparing the DLIT and EL images recorded close to the operating point of the cells under full shading (virgin-grade cell: V ≈ -12.75 V, I ≈ 8 A, Fig. 9f and g; umg cell: V ≈ -9.75 V, I ≈ 8 A, Fig. 9k and l) shows, that the cells do not suffer from severe local shunting but are dominated by junction breakdown (very simplified: breakdown spots emit radiation detectable with EL and DLIT and ohmic shunts radiation only detectable by DLIT and can therefore be separated). Hence, they are well suited to investigate the hot spot potential of breakdown mechanisms in mc-Si.

Figure 9a shows the voltage-dependent local current density, that can be extracted from DLIT measurements [21], for three spots on the virgin cell marked in Fig. 9f. The characteristic ohmic behaviour of type I breakdown, soft breakdown behaviour of type II breakdown and hard breakdown behaviour of type III breakdown can be found exemplary in these three spots. Although located on the edge of the cell, spot I can be attributed to type I breakdown because it also exhibits an EL signal in reverse, see Fig. 9g. The type II breakdown spot is at a site of recombination active dislocations as can be seen from the forward EL image in Fig. 9h, and the type III breakdown spot at a site without recombination active defects. Hence, the "classical" mechanisms as proposed by Kwapil [2] and Breitenstein [1] seem to be present on the investigated cells (similar sites can be identified on the umg cell).

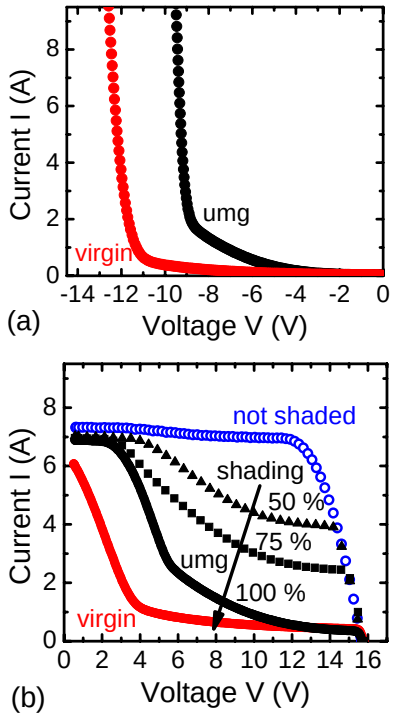

Figure 8: (a) Measured dark cell IV curves under reverse bias of investigated umg and virgin-grade cell. (b) Module IV characteristics recorded for different shading scenarios in during hot spot testing (thermal chamber with $T_{module} \approx 50°C$).

3.3 Hot spot test

The module is tested on hot spots in the thermal chamber which is used for module certification at Fraunhofer ISE Testlab PV Modules. The module is irradiated with lamps giving a uniform AM1.5G spectrum with an intensity $I \approx 1000\ W/m^2$ across the entire module area. The chamber is temperature controlled so that the module temperature under open-circuit conditions is approximately 50°C. This setup is compliant to the required test conditions during module certification [14, 15].

The applied test procedure is as follows: The IV characteristic of the module is measured unshaded, then the investigated cell is shaded to the desired ratio and the module IV characteristic recorded again. Afterwards, the module is short-circuited and the temperature monitored with an IR camera facing the backsheet of the module. Once the maximum hot spot temperature gets into a critical regime and damage to the module encapsulation system becomes visible, the measurement is aborted. The critical temperature for the module encapsulation, where discolouring and delamination starts, was determined during the measurements to be in the range of $T_{critical} = 150$ to 190°C.

First, the behaviour of the virgin-grade cell is discussed. Figure 8b shows the IV characteristic of the test module unshaded and with the virgin-grade cell being fully shaded. As can be seen in Fig. 9b, the maximum temperature of the cell moderately increases up to a shading time of approximately t = 11 min. Then, suddenly a steep increase in maximum temperature occurs which leads to a visible damage of the module encapsulation. The temperature distribution across the shaded cell first follows the distribution of the DLIT signal in Fig. 9f not leading to critical temperatures, but then shifted to the right edge of the cell as shown in Fig. 9i. The final steep increase in maximum temperature was due to the activation of a mechanism on the right edge of the cell, marked by the cross in Fig. 9i. Interestingly, the detrimental hot spot does not coincide with the location of maximum local power dissipation determined by DLIT, which dominates the heat dissipation in the first eleven minutes of the shading experiment.

Figure 9c depicts the development of the maximum hot spot temperature in another cell, which qualitatively exhibits the same behaviour but on a different time scale. As for the virgin-grade cell, the heat distribution first follows the DLIT signal but then concentrates on the edge leading to module damage. Comparing Fig. 9b and c shows, that the edge effect leading to module damage seems not to be time- but temperature-activated at a temperature of T ≈ 160°C. This behaviour was similarly observed on more cells, e.g., also on the cell manufactured from the industrial reference wafers, and sometimes appeared for different shading ratios.

Figure 8b shows the module IV characteristics for the shading scenarios applied to the umg cell. As expected from the simulations, the IV characteristic is shifted by the photo-generated current in the partially shaded cell. For 50 % shading, three different halves of the cell have been shaded leading to identical module characteristics. It can be seen, that the power output of the module is higher for shading the umg cell than shading the virgin-grade cell due to the lower breakdown voltage of the umg cell. Figure 9d shows, that for 100 % shading, the maximum hot spot temperature saturates after t = 16 min at an

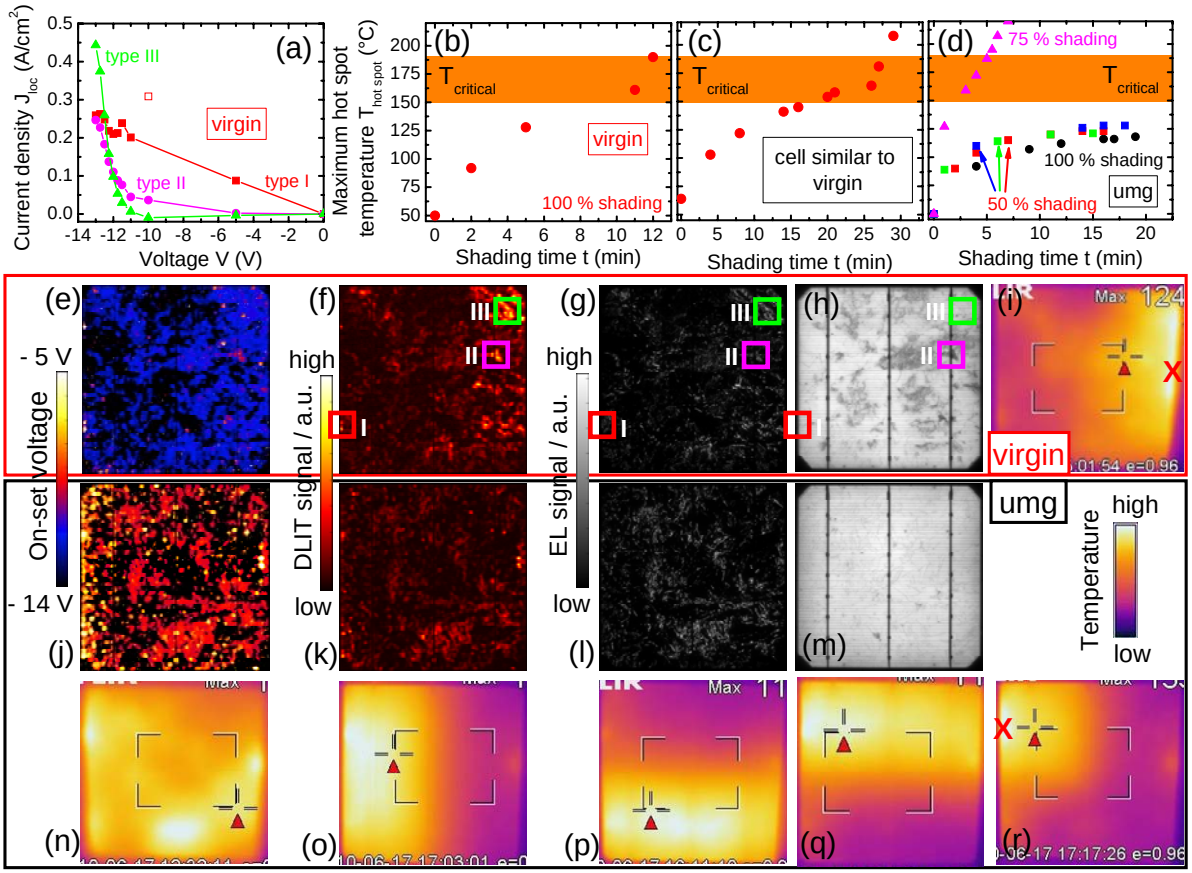

Figure 9: (a) Local JV characteristic of type I, II and III breakdown sites on virgin-grade cell, see (f). **(b)-(d)** Maximum hot spot temperature of virgin-grade cell, similar cell to virgin-grade cell and umg cell. **(e)-(i)** Virgin-grade cell: On-set voltage map, DLIT and reverse EL ($V \approx -12.75$ V, $I \approx 8$ A), EL under forward bias and IR image of cell while being 100 % shaded. **(j)-(m)** Umg cell: On-set voltage map, DLIT and reverse EL ($V \approx -9.75$ V, $I \approx 8$ A) and EL under forward bias. **(n)-(r)** IR images of the umg cell being from left to right (n) 100 % shaded, (o) right half 50 % shaded, (p) top half 50 % shaded, (q) bottom half 50 % shaded and (r) right and bottom half shaded resulting in 75 % shading. The highest temperatures are observed in the illuminated part of the partially shaded cell.
On-set voltage maps, DLIT, EL and IR images are oriented analogously; **X** marks the position of the edge effect leading to a detrimental hot spot.

uncritical temperature of $T_{hot\ spot} \approx 120$°C. Moreover, the heat distribution in the shaded cell correlates closely to the spatially resolved DLIT signal, as can be seen from a comparison of Fig. 9n and k. The shift of the maximum heat dissipation to the edge has not been observed, contrary to the results on the virgin-grade cell. Figures 9o–q show the heat distribution for partially shading the right, upper and lower halves of the cell, respectively. The temperature is highest in the illuminated part of the cells which is expected from the simulation results of subsection 2.2.3. Interestingly, the power dissipation increase due to illumination, which is predicted by the simulations, dominates the junction breakdown mechanisms. For example, the dominant breakdown site in the bottom middle of the cell, which is dominant in the IR image under full shading in Fig. 9n also dominates if it lies within the illuminated part of the cell (see Fig. 9p). However, this site is completely dominated by illuminated parts of the cell even if these parts do not break down when being located within the dark part of the partially shaded cell (see Fig. 9q). For all three applied 50 % shading scenarios, the maximum hot spot temperature behaves similarly and is below the critical range, as shown in Fig. 9d. For 75 % shading, the power dissipation concentrates in the illuminated top left part of the cell, see Fig. 9r. This leads to a significantly higher hot spot temperature which causes module damage after $t \approx 5$ min. The temperature behaviour is similar to the one of the virgin cell under full shading, i.e., the spot of maximum temperature shifts to the edge of the cell leading to a steep increase once 160°C are reached.

3.4 Summary module test

Table I displays the summary of the performed hot spot experiments. Some cells fail the test while being fully shaded, some do not until being partially shaded. However, all cells investigated under partial shading conditions could be pushed into an operating point where module damage occurred.

The hot spot experiments can be summarized as followed:

(1) The dominant junction breakdown mechanisms of the investigated cells (including type I, II and III breakdown) which were imaged by state-of-the-art breakdown characterization techniques such as DLIT and EL have not led to hot spots in the assembled test module. One reason might be, that the breakdown spots are evenly distributed across the cell plane.

(2) All observed hot spots were due to an effect at the edge which was activated at approximately 160°C.

Table I: Summary of the hot spot experiments. The numbering of the cells is from bottom to top in the respective ingots. ✓ = hot spot test passed, ✖ = hot spot test failed.

	Virgin					**Umg**														**Ref**
Cell ID	1	2	3	4	5	1	2	3	4	5	6	7	8-13	14	15	16	17	18-20	21	22	1
Full shading		✓	✓	✓	✖	✖	✓		✓	✓	✖	✖		✖	✓		✓		✓	✓	✖
Partial shading		✖	✖						✖	✖		✖					✖				

Before its activation, the local heat dissipation in the investigated cells followed the distribution of the DLIT signal. Once activated, the edge effect took over most of the power dissipation leading to a steep increase in hot spot temperature and irreversible module damage. If the temperature of a shaded cell stayed below 160°C, the edge effect was never activated, not even for long shading times of t >25 min.

(3) The edge effect occurred at different locations and under different shading conditions for the investigated cells. The position where the effect occurred was localized on each cell and did not coincide in the different cells. This makes a systematic processing or crystal growth problem unlikely. Its location never coincided with the regions of maximum DLIT signal. Note that the thermal characteristics of the encapsulation system of a solar module significantly differ from the environment during cell characterization.

(4) Every investigated cell could be pushed to an operating point where the thermal edge effect was activated.

(5) There was no significant difference in hot spot behaviour between cells from virgin-grade and umg feedstock observed.

(6) The illuminated part always exhibited higher temperatures than the dark part of a partially shaded cell independently of the position of the dominant hot spot under full shading conditions. This is due to the photo-generated current acting in the same direction as the current under reverse bias and leading to a significant increase in power dissipation in the illuminated part and a decrease in the dark part of the cell, as discussed in subsection 2.2.3.

(7) No measurable multiplication of breakdown was observed in the illuminated part of the cell, which might be expected for avalanche-like breakdown. The theoretically expected lower power loss during shading for a cell with lower breakdown voltage is experimentally verified.

4 SUMMARY AND CONCLUSION

Within this paper, the operating point and power dissipation of two representing solar cells in a standard industrial module were modelled for different shading scenarios. It was shown, that bypass diodes only moderately limit the power dissipation in voltage-limited cells to about a third of the maximum module output power (for modules with three incorporated bypass diodes). This power can be dissipated in every cell (even when exhibiting very low currents under the applicable reverse bias) for a specific shading ratio. Cells that break down before incorporated bypass diodes turn on can even exhibit a lower maximum power dissipation, especially in the illuminated part. At the same time, shading those current-limited cells can lead to a smaller loss in maximum module output power.

The frequently cited argument that cells which break down under reverse bias while being shaded in a solar module suffer from a higher total power dissipation than cells which do not break down therefore seems unreasonable. This argument only holds for full but not for partial shading. Frequently, the opposite is true.

After having clarified, that junction breakdown does not have to be “bad” with respect to total power dissipation but can even be beneficial, the local distribution of the power dissipation under the operating conditions in a module is investigated on mc-Si solar cells from wafers cut and crystallized from different types of Si feedstocks, including umg-Si. Solar cells exhibiting the prominent established breakdown mechanisms were identified and built into a test module for a test on hot spots behaviour.

For the tested cells, none of the dominant breakdown mechanisms identified during characterization on cell level has led to detrimental hot spots. However, a newly observed effect at the edges, which was thermally activated at around 160°C after a significant shading time, damaged all investigated cells. Hence, for a comprehensive investigation of hot spots on cell level, also effects, that do not appear up to a certain shading time have to be taken into account in addition to effects which are detected by traditional breakdown analysis techniques such as DLIT and EL. Furthermore, the simulation result that the illuminated part dominates the dark part of a partially shaded cell could be confirmed experimentally even if breakdown mechanisms which are dominant under full shading are located in the shaded part of the cell. These effects that are relevant under realistic module operation should be considered for future breakdown experiments.

The argument that full junction breakdown is always critical to form hot spots in solar modules seems not to be true. It appears that if the breakdown spots are spatially distributed over the cell plane, they might be tolerable. However, the underlying mechanisms leading to the ovserved edge effect have to be further investigated and eliminated in order to ensure safe module operation. If this is successfully done, solar cells with lower breakdown voltages such as cells from umg feedstock can be used without concerns in standard modules possibly enabling a wider use of cheaper umg-Si. The use of these cells would lead to a lower loss in a module’s output power when cells are shaded. Since bypass diodes in a standard setup do not turn on for cells with sufficiently low breakdown voltages, they can be eliminated enabling novel module designs.

6 ACKNOWLEDGEMENTS

We would like to thank all co-workers at Fraunhofer ISE for crystallization, wafering, cell and module processing and especially J. Greulich for support in programming. This work has been supported by internal project funding of the Fraunhofer Society.

7 REFERENCES

[1] O. Breitenstein et al., in *Proceedings of the 34th IEEE PV Specialists' Conference*, (Philadelphia, USA, 2009).
[2] W. Kwapil et al., *Journal of Applied Physics*, **106**: p. 063530, (2009).
[3] D. Lausch et al., *Applied Physics Letters*, **97**: p. 073506, (2010).
[4] W. Kwapil et al., *Applied Physics Letters*, **95**(232113): p. 1-3, (2009).
[5] J. Bauer et al., *Physica Status Solidi RRL*, **3**(2): p. 40-2, (2009).
[6] W. Kwapil et al., *Journal of Applied Physics*, **108**: p. 023708, (2010).
[7] V. Hoffmann et al., in *Proceedings of the 23rd EUPVSEC*, (Valencia, Spain, 2008).
[8] S. Wendlandt et al., in *Proceedings of the 25th EUPVSEC*, (Valencia, Spain, 2010).
[9] M. Danner et al., in *Proceeding of the 26th IEEE PV Specialists' Conference*, (Anaheim, USA, 1997).
[10] J. W. Bishop, *Solar Cells* **25**, 73 – 89, (1988).
[11] V. Quaschning, *Simulation der Abschattungsverluste bei solarelektrischen Systemen.* Thesis, (Dr. Köster, Berlin, 1996)
[12] A. Woyte et al., *Solar Cells* **74**, 217–233, (2003).
[13] M.C. Alonso-Garcia et al., *Solar Energy Materials & Solar Cells* **90**, 329-340, (2006)
[14] *International Standard IEC 61215: Crystalline silicon terrestrial photovoltaic (PV) modules – Design qualification and type approval*, International Electrotechnical Commission, 2nd edition (2005).
[15] *UL Standard for Safety for Flate-Plate Photovoltaic Modules and Panels, UL 1703* – Underwriters Laboratories Inc., 3rd edition (2002).
[16] A. Goetzberger et al., *Sonnenenergie: Photovoltaik.* (Teubner, Stuttgart, 1997).
[17] S.R. Wenham et al., *Applied Photovoltaics*. (Earthscan, London, 2007)
[18] S. Riepe et al., in *Proceedings of the 23rd EUPVSEC*, (Valencia, Spain, 2008).
[19] D. Biro et al., in *Proceedings of the 21st EUPVSEC*, (Dresden, Germany, 2006).
[20] M. Wagner et al., in *Proceedings of the 24th EUPVSEC*, (Hamburg, Germany, 2009)
[21] O. Breitenstein et al., *Lock-in Thermography*. (Springer, Berlin, 2010).